

CHEMISTRY

A **European** Journal

A Journal of



Accepted Article

Title: A constrained and “inverted” [3 + 3] salphen macrocycle with an ortho-phenylethynyl substitution pattern

Authors: Tomas Torres and Maxence Urbani

This manuscript has been accepted after peer review and appears as an Accepted Article online prior to editing, proofing, and formal publication of the final Version of Record (VoR). This work is currently citable by using the Digital Object Identifier (DOI) given below. The VoR will be published online in Early View as soon as possible and may be different to this Accepted Article as a result of editing. Readers should obtain the VoR from the journal website shown below when it is published to ensure accuracy of information. The authors are responsible for the content of this Accepted Article.

To be cited as: *Chem. Eur. J.* 10.1002/chem.201904763

Link to VoR: <http://dx.doi.org/10.1002/chem.201904763>

Supported by
ACES

WILEY-VCH

A constrained and “inverted” [3 + 3] salphen macrocycle with an *ortho*-phenylethynyl substitution pattern

Maxence Urbani^{*[a,b]} and Tomas Torres^{*[a,b,c]}

Abstract: A novel [3+3] Schiff base salphen macrocycle (**7a**) was synthesized by imine condensation between *ortho*-phenylenediamine and *ortho*-phenylethynyl-bridged bis(5-salicylaldehyde) precursors. The triangular-shaped macrocycle **7a** has a non-classical design (or “inverted”), with the N₂O₂ coordination “pockets” located at the sides instead of corners. **7a** could be synthesized in a reasonably good yield (64%) considering the steric constraints imposed by the *ortho*-substitution pattern. Subsequent zinc-metalation afforded the corresponding Zn-metallomacrocycle **7b**. Spectroscopic experiments evidenced weak (**7a**) to strong (**7b**) self-aggregation behaviour in solution. Their ability to self-organize at the supramolecular level was further studied in the solid state by AFM and TEM experiments, revealing the formation of large bundles of fibers with lengths of several microns and width of nanometers.

Introduction

Schiff base ligands have been widely explored for the preparation of stable and functional coordination complexes, and have raised interest in various fields of research, especially in catalysis^[1] and asymmetric catalysis^[2], but also as colorimetric sensors triggered by metal–ligand coordination,^[3] crystalline porous materials (CPMs),^[4, 5] molecular magnets,^[6] liquid crystals^[7–10] and energy materials^[11] including organic light emitting diodes (OLED)^[12, 13] and also more recently dye-sensitized solar cells (DSSC).^[14] They are distinguished by their relative ease of synthesis (condensation between carbonyl and primary-amine precursors), and tuneable denticity allowing multiple-binding of several kinds of metal ions, thus offering a large panel of oxidation state, tuneable optical, redox, and even magnetic properties of their metal complexes.^[15] Salen is a large family of tetradentate Schiff base ligands prepared by condensation between hydroxy-benzaldehyde and primary-diamine precursors. The cooperative metal-binding effect owing to their N₂O₂ pocket makes them powerful ligands for metal complexation. Salphens are π -conjugated salen systems, thus holding several advantages in terms of stability, optical

properties and reactivity, making them excellent catalyst and ion-sensors for instance. Remarkably, mononuclear Zn(II) Schiff-base complexes are known to form dimeric structures having a typical Zn₂O₂ central unit, mediated by strong intermolecular Zn–O coordinative interactions (through μ -2-phenoxo bridging).^[16–18] Salphen-type macrocycles have attracted a particular interest in the field of supramolecular chemistry, owing to their ability to self-assemble into organised stacks.^[7–10, 19–21] In particular, the aggregation behaviour of multinuclear Zn(II) salphen complexes is strongly enhanced owing to their unusual oligomeric (Zn–O)_n coordination motifs, a peculiar property that has been exploited for the construction of self-assembled nanostructures of very high stability.^[18, 22–24]

The reversibility character of the imine condensation within dynamic exchange of C=N bonds meets the requirements for dynamic covalent reactions,^[25] which has been exploited to prepare shape-persistent 2D and 3D molecular systems of high-complexities and in high yields, such as macrocycles^[26–30] tiered-architectures,^[31] capsules^[32] and molecular cages.^[33–38] One of the main synthetic challenge is to obtain selectively one type of macrocycle within a given size and in good yield. For this purpose, the most convenient and efficient method to prepare symmetrical salphen macrocycles involves the condensation between a diformyl-aromatic precursor and *ortho*-phenylenediamine derivative in a one pot-synthesis. Initially, one of the first reports relied on the condensation between 3,6-diformylcatechol and *ortho*-phenylene diamine producing almost exclusively a triangular and shaped-persistent [3+3] macrocycle and in remarkable high yield (up to 91%).^[39, 40] Latter on, incorporation of different linear spacers into their backbone allowed to access macrocycles with tuneable size and optical properties, as for instance, phenyleneethynylene linkers pioneered by MacLachlan and co-workers.^[41] By changing the geometry (length, curvature) and/or nature of the diformyl-aromatic precursor, several macrocycles of different size and shape could be prepared in high yields following a similar strategy: [3+3],^[41–45] [4+4],^[7–9] and [6+6].^[46] Several examples of soluble triangular-shaped [3+3] Schiff-base macrocycle of different size have been reported, including salen (triangleimine) and salphen types.^[41–44] Nonetheless, it is worth to notice that all of them are constructed in a similar fashion, that is by condensation of a bis(4-substituted-2-hydroxybenzaldehyde) precursor (linearly linked) and an *o,o*-substituted diamino derivative. Consequently, they possess the three N₂O₂ pocket coordination sites located at each corners of the triangle (Chart 1.a, left). To our knowledge, the only example of a [3+3] salphen-type macrocycle with an “inverted configuration”, that is three N₂O₂ pocket located at the sides instead of corners of the triangle (Chart 1.b, right), was reported by MacLachlan and co-workers.^[47] In their work, two macrocycles with regioisomeric backbones were reported, one constructed in a classical way and the other one in a non-

- [a] Dr. M. Urbani, Prof. T. Torres
Departamento de Química Orgánica, Universidad Autónoma de Madrid, Cantoblanco, 28049 Madrid, Spain
E-mail: maxence.urbani@uam.es, tomas.torres@uam.es
- [b] Dr. M. Urbani, Prof. T. Torres
IMDEA-Nanociencia, Campus de Cantoblanco, 28049 Madrid, Spain
- [c] Prof. T. Torres
Institute for Advanced Research in Chemical Sciences (IAChem)
Universidad Autónoma de Madrid, 28049 Madrid, Spain.

Supporting information for this article is given via a link at the end of the document.

conventional (or inverted) fashion. To achieve such designs, two isomeric 2-hydroxy-benzaldehyde (or salicylaldehyde) units substituted either at the 4- or 5- position, were attached to a linear- (180°) or a 60° - linker, respectively, and subsequently condensed with the same diamino precursor. Most importantly, they observed drastic differences regarding their aggregation behaviour, one regioisomeric macrocycle being strongly aggregated in solution whereas the other one was not (or weakly), which they ascribed to what they called “social or antisocial” arrangement. In this work, we report the synthesis of a novel triangular-shaped [3+3] Schiff base salphen macrocycle (**7a**) constructed in a non-conventional fashion (inverted) and having an *ortho*-type substitution pattern, and subsequent Zn-metallation into metallomacrocycle **7b**. These macrocycles display weak - (**7a**) to strong- (**7b**) tendency to undergo aggregation in solution as supported by NMR and UV-visible spectroscopy experiments. The ability of these macrocycles to self-organize at the supramolecular level was further studied in the solid state by AFM and TEM experiments.

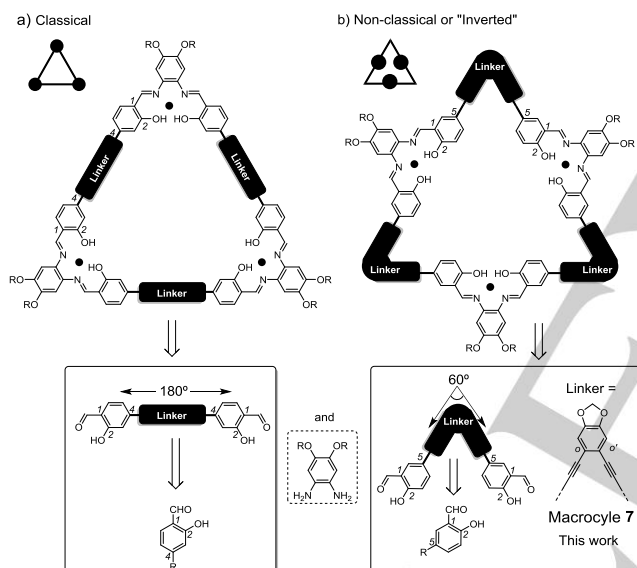
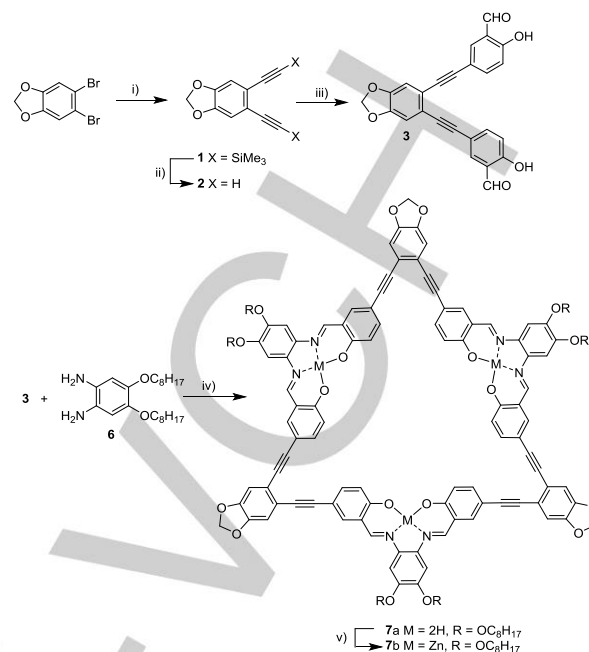


Chart 1. Schematic representation of triangular-shaped [3+3] Schiff base macrocycles with regioisomeric backbones (note the 1,2,4 and 1,2,5 isomeric positions); black dots represent the location of the coordination sites, so-called “salphen pockets”.

Results and Discussion

Synthesis

The synthesis of macrocycle **7a** relies on an imine condensation between a di-salicylaldehyde precursor (**3**) and 4,5-bis(octyloxy)benzene-1,2-diamine (**6**) (Scheme 1). Detailed synthesis and characterization of the precursors are provided in the Supporting Information. The conditions of reaction for the formation of the [3+3] macrocycle were found crucial. Initially, several conditions were unsuccessfully attempted to obtain **7a**:

in mixtures of solvents $\text{CHCl}_3/\text{EtOH}$ (1:1), AcCN/EtOH (2:1), or $\text{CHCl}_3/\text{AcCN}$ (8:2), at reflux for 1–2.5 days and concentration of reagents ($[\mathbf{3}] = [\mathbf{6}] = 1 \text{ mM}$ or 12 mM). Under these conditions, we systematically obtained intensively colored crude of reactions (orange/red) fully soluble in common organic solvent (e.g.: CHCl_3). However, MS and ^1H NMR analysis of these crudes revealed complex mixtures of open-forms (oligomers) and/or macrocycles in various proportions, with only traces of the desired [3+3] macrocycle. The identified macrocycles by MS analysis were the [1+1] as the major product, followed by [2+2], [3+3], [4+4] as minor products. Changing the conditions to a refluxing mixture of $\text{CHCl}_3/\text{AcCN}$ (1:1) at ca. $85\text{--}90^\circ\text{C}$ for 24 h, and a concentration of 12 mM ($[\mathbf{3}] = [\mathbf{6}]$), we observed this time the formation of an orange precipitate during the course of the reaction as the major product. MS analysis of the insoluble fraction identified the [3+3] macrocycle, confirming its successful formation under these conditions, while that of the supernatant (fully soluble material) revealed the presence of the [1+1] and [2+2] macrocycle as major products (see Figures S3 and S4 in the ESI). In fact, **7a** is poorly soluble in most of common organic solvents despite the presence of six peripheral octyl chains (ca. $1.5\text{--}2 \text{ mg/ml}$ in CHCl_3). Based on the geometry-optimized structures (see ESI, Table S1), only the [3+3] macrocycle **7a** should be able to adopt a conformation with enough planarity to allow aggregation by $\pi\text{-}\pi$ stacking (Figure 1), which should not be possible for the smaller [1+1], [2+2] and larger [4+4] ones. This explains well why experimentally, oligomers (open-forms) and mixture of macrocycles ([1+1], [2+2] and [4+4]) were soluble in the crude (supernatant), while the [3+3] one (**7a**) precipitate

during the course of the reaction. As Zhang and Moore^[28] discussed in details for a typical [3+3] salphen macrocycle reported by MacLachlan and collaborators,^[41] the [3+3] one should be, in principle: 1) enthalpically favored over the smallest [1+1] and [2+2] ones because of less angle strain, and 2) entropically favoured over the larger [4+4] ring. Geometry-optimized structure predicted by DFT calculations suggests that **7a** is able to adopt a pseudo-planar configuration (though relatively distorted) despite the steric repulsion between the inner CH-phenylene protons (see Figure 1). The above results and experimental observations, suggest that the formation of macrocycle **7a** might not be solely thermodynamically-driven but also governed by solubility (precipitation of the aggregates). Under optimal conditions, **7a** was obtained in a reasonable 64% yield, which lies in the range of reported values for [3+3] Schiff-base macrocycles (40–90%).^[42–44] Finally, the zinc-metallomacrocycle **7b** was obtained by metalation of **7a** with an excess of Zn(OAc)₂ (3.4 eq) in THF/EtOH (4:1) at 45 °C for 2.5 h.

NMR and UV-visible spectroscopy

As commented before, **7a** displays a relative poor solubility in most common organic solvents and tend to precipitate progressively in solution after relatively short period of times, indicative of aggregation. Thus, it rendered difficult characterization by NMR since poor solubility and tendency to undergo aggregation imposed to work at low concentration. At a concentration below ca. 1 mM, a well-defined ¹H NMR spectrum of **7a** in CDCl₃ solution could be recorded (Figure 2), showing in particular, a unique single singlet signal for both the phenolic (upshifted at $\delta_{\text{H}} = 13.39$ ppm) and iminic ($\delta_{\text{H}} = 8.32$ ppm) protons, characteristic of the salphen pocket. ¹H NMR spectra of **7a** were also recorded in d₈-THF and d₆-DMSO solutions (see Figures S26, S72 and S73 in the ESI). In d₈-THF, the solubility was slightly improved but no significant differences were observed in the NMR spectrum with respect to that recorded in CDCl₃. The ¹H NMR spectrum of **7a** in dilute d₆-DMSO solution (0.75 mM) was much less resolved than in CDCl₃ or d₈-THF but is qualitatively the same with the exception of the quasi-disappearance of the PhOH protons signals, similarly than observed in a 9:1 mixture d₈-THF/d₄-MeOH. At higher concentration (1–2 mM) in d₆-DMSO, the NMR spectrum is much less resolved and **7a** precipitate reatively quickly (<1 h). In very polar solvent such as DMSO, the intramolecular H-bonding in **7a** should be disrupted, however no change was observed regarding the solubility or NMR features. These results suggest that π - π stacking is the dominant interaction towards the self-assembly of the metal-free macrocycle **7a**.

UV-visible absorption spectroscopy experiments in solution did not reveal any spectral changes for **7a** in the 250–2 $\mu\text{mol/l}$ concentration range (either in CHCl₃ or THF), which support that **7a** is fully disaggregated in solution below 1 mM, and moreover, is not affected by the nature of the solvent (see Figures S34–S38 in the ESI).

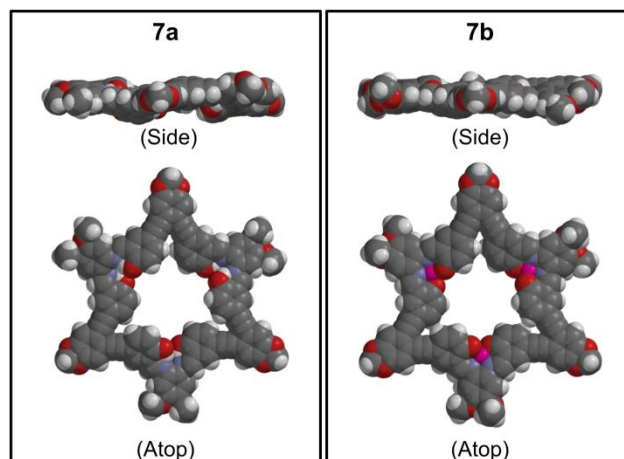


Figure 1. Geometry-optimized structures of **7a** and **7b** in vacuum predicted with DFT calculations at the B3LYP (6-31G*) level of theory (*n*-octyl chains have been replaced by methyl groups in the calculations; grey: carbon, white: hydrogen, red: oxygen, blue: nitrogen, and pink: zinc atoms).

To further support that the observed ¹H NMR spectra of **7a** at low concentration range (1 mM) does correspond to the monomeric species in solution and, in addition, to estimate the size of the macrocycle, DOSY ¹H NMR experiments were performed both in CDCl₃ and d₈-THF solutions. As exemplified for the 2D-DOSY spectrum of **7a** in d₈-THF depicted in Figure 3, the NMR signals belong to a unique specie diffusing in solution, with average diffusion coefficients (*D*) ranging from 4.4–4.7 × 10⁻¹⁰ m²/s in d₈-THF to 4.6–5.1 × 10⁻¹⁰ m²/s in CDCl₃ (see Figures S28–S31 in the ESI). It is worth to notice that the phenolic protons signal systematically gave slightly greater diffusion coefficient values (+ 5–10%) than the other ones, which can be reasonably explained by PhOH-imine proton-exchange phenomena.^[48] Given the experimental margin errors for the determination of the absolute values of diffusion coefficients, DOSY spectra were also recorded in the presence of mesitylene as internal reference, in order to better estimate the hydrodynamic radius of the macrocycle. Mean values of 15±1 Å from d₈-THF and 13.0 ± 0.7 Å from CDCl₃ were extracted from the DOSY experiments, which match fairly well the 15.6 Å molecular radius estimated from the DFT geometry-optimized structure (Figures S32 and Table S3 in the Supporting Information). Surprisingly, **7b** was noticeably more soluble in organic solvent than its analogue **7a**, and did not precipitate in time at the same concentration used for NMR analysis (ca. 1 mM). In all ¹H NMR spectra recorded for **7b**, the phenolic proton singlet signal (characteristic of the metal-free macrocycle) was clearly absent, as expected if three zinc metals are bounded to the tridentate macrocycle ligand through the N₂O₂ coordination sites. However, very broad and ill-defined NMR spectra were systematically obtained for this compound (CDCl₃ or d₈-THF; see Figure S27), which, as it can be anticipated, indicate that **7b** is readily and strongly aggregated in solution at the NMR concentration. Zinc-multimetallic salphen complexes are indeed well-known to strongly self-assemble through oligomeric (Zn–O)_{*n*} coordination motifs with very high-stability.^[22,23]

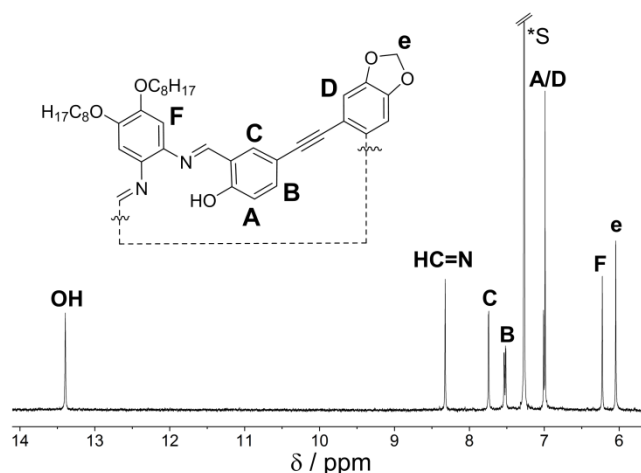


Figure 2. Partial ^1H NMR spectrum (400 MHz; 298K) of **7a** in CDCl_3 solution ($[\mathbf{7a}] < 1 \text{ mM}$); *S denotes the residual CHCl_3 solvent peak).

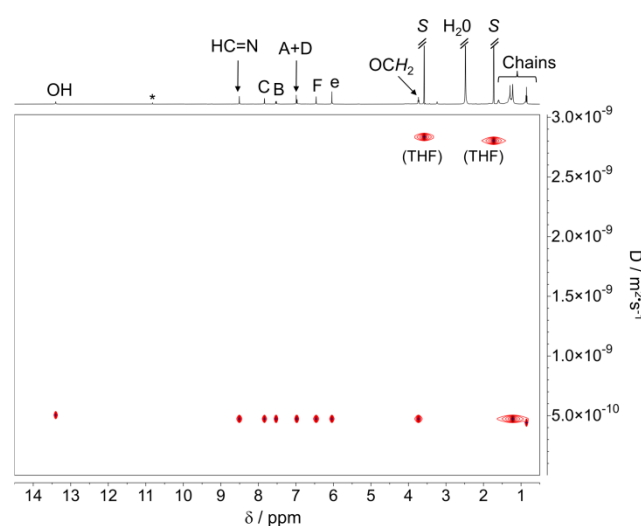


Figure 3. 2D-DOSY ^1H NMR (500 MHz; 298 K) spectrum of **7a** in $\text{d}_8\text{-THF}$ solution ($[\mathbf{7a}] < 1 \text{ mM}$); S denote the residual signals of the THF solvent (for nomenclature of the protons, see Figure 2); * denotes the signal of a recurrent and residual impurity of the employed commercial $\text{d}_8\text{-THF}$ solvent (see Figure S26 in the Supporting Information for details).

In fact, UV-visible absorption spectroscopy experiments in solution (Figures 4 and S45-S60 in the ESI) revealed that **7b** is fully aggregated at concentrations as low as $2 \mu\text{mol/L}$ in low-polar solvent (CHCl_3 or CH_2Cl_2). Aggregation-disaggregation of **7b** was observed by UV-Visible absorption spectroscopy at variable concentration (Figures 4.A,B) and by spectroscopic titration with pyridine (Figures 4.C,D). Remarkably, even a large excess of pyridine ($>10,000 \text{ Eqs}$) was not sufficient enough to desaggregate entirely **7b** in CHCl_3 , and this, even at concentration below $10 \mu\text{mol/L}$ (Figure 4.C and S54).

In more polar and disaggregative solvent, such as THF, **7b** is fully desaggregated at a concentration of $12 \mu\text{mol/L}$ (see Figures 4.B,D), and start to aggregate at around $30 \mu\text{mol/L}$ (Figure S57 in the ESI). As well, aggregation-disaggregation was also observed at low concentrations (9 mM) in mixtures of CHCl_3 and THF solvents (see ESI, Figure S58).

These results evidence that **7b** is strongly aggregated through oligomeric $(\text{Zn-O})_n$ coordination motifs, in contrast to the weakly aggregated macrocycle **7a** for which $\pi\text{-}\pi$ stacking is the dominant interaction. It is worth to notice that at concentrations of 0- and $\text{above-}1 \text{ mM}$, **7b** is still perfectly soluble in organic solvent (e.g. CHCl_3) despite being fully aggregated, whereas **7a** readily precipitate above this concentration. The proposed structure of both macrocycles was confirmed by MALDI-TOF mass spectrometry. The MS spectrum of **7a** shows a unique signal corresponding to the molecular ion peak ($[\mathbf{7a}]^{*+}$) at $m/z = 2216.1$, and without detection of dimeric species. In turn, the most intense one for **7b** corresponds to the dimer ($[(\mathbf{7b})_2]^{*+}$) at $m/z = 4813.7$ rather than that of the monomer specie ($[(\mathbf{7b})]^{*+}$) at $m/z = 2405.8$, which supports the strong aggregation character of the zinc-metallomacrocycle (see Figures S6-S9 in the ESI).

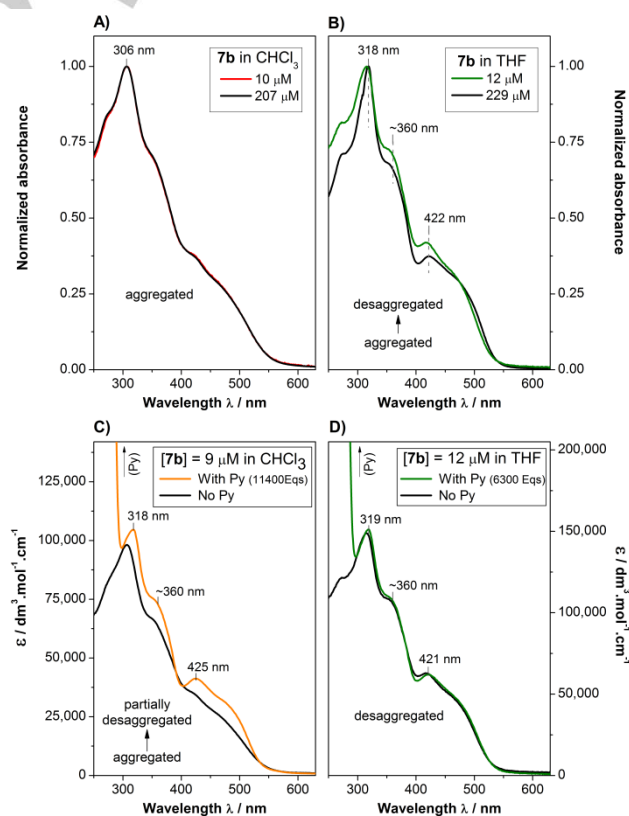


Figure 4. Effect of the concentration (A,B) and pyridine (C,D) toward aggregation behavior of **7b**: UV-visible absorption spectra of **7b** in A), C) CHCl_3 and B),D) in THF solutions.

The UV-visible absorption spectrum of the metal-free macrocycle **7a** in THF solution (14 μM ; Figure 5), shows an intense absorption in the UV region but only a modest one in the visible range (above 400 nm). Upon addition of three equivalents of $\text{Zn}(\text{OAc})_2$, the whole absorption spectrum was significantly redshifted, in addition to the appearance of a relatively strong absorption band in the visible region ($\lambda_{\text{max}} = 420 \text{ nm}$), extending up to ca. 550 nm. In the emission spectra, it can be remarked an important blue-shift ($\Delta\lambda_{\text{max}} = 50 \text{ nm}$) of the emission band, from 595 nm to 545 nm after addition of the zinc metal salt. Absorption and emission spectra of the as synthesised zinc-metallomacrocycle **7b** match those obtained from titration experiments of **7a** with $\text{Zn}(\text{OAc})_2$ (Figure 5). Redshift of the absorption spectrum accompanied with appearance of a strong absorption band in the visible region, and shorter Stoke shifts may be indicative of a gain in planarity and hence a more effective conjugation for the zinc-metallo (**7b**) with respect to the metal-free (**7a**) macrocycle. Geometry-optimized structures support this hypothesis since **7b** is fairly more planar than **7a** (Figure 1). To further confirm the structure of **7a**, and therefore the three available metal- coordination sites present in the [3+3] macrocycle, UV-Visible absorption (Figure 6) and luminescence (see ESI, Figures S43-S44) spectrophotometric titrations of macrocycle **7a** with $\text{Zn}(\text{OAc})_2$ were performed in THF solutions. The corresponding Job's plot analyses support that macrocycle **7a** is indeed able to coordinate three zinc-metal centers into its cavities (*i.e.* ratio $[\mathbf{7a}]/[\text{Zn}]$ of 1:3). UV-visible absorption and fluorescence spectroscopic experiments show the ability of **7a** to bind various other metals after addition of an excess (3–4 eq) of the corresponding acetate metal salt at rt ($\text{M}(\text{OAc})_2$, with $\text{M} = \text{Co}, \text{Cu}, \text{Ni}, \text{Mg}$ and Mn ; see Figures S69-S71 in the Supporting Information). In this work, we focused on zinc-metallomacrocycle (**7b**) owing to its well-known and peculiar property to strongly self-assemble (through Zn-O interactions) and present also the advantage to be highly soluble in organic media even when strongly aggregated.

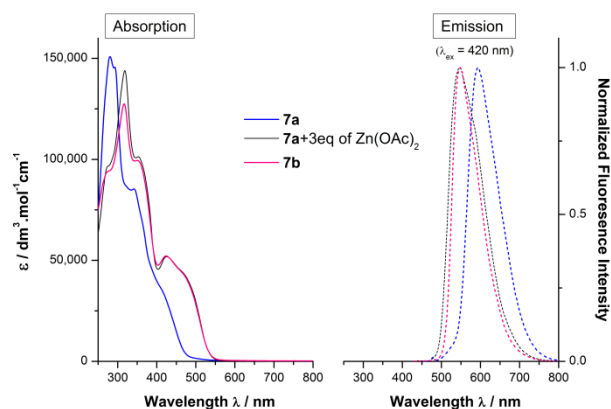


Figure 5. UV-Visible absorption (solid lines) and emission (dashed lines; $\lambda_{\text{ex}} = 420 \text{ nm}$) spectra in THF solutions of metal-free macrocycle **7a** (blue lines), **7a**+ $\text{Zn}(\text{OAc})_2$ (3 eq.) (black lines), and as synthesised zinc-metallomacrocycle **7b** (pink lines); with $[\mathbf{7a}] = [\mathbf{7b}] = [\text{Macrocycle}]_{\text{total}} = 14 \mu\text{M}$.

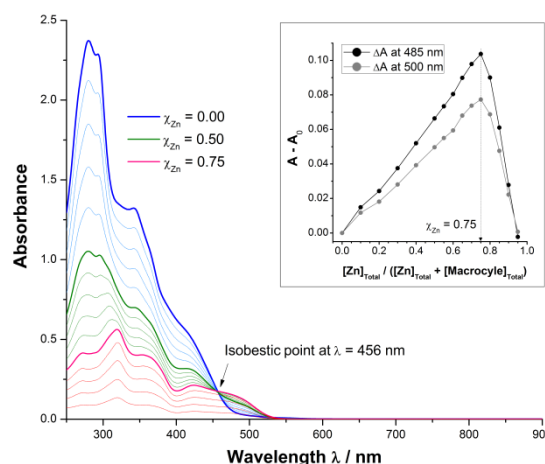


Figure 6. UV-Visible absorption spectrophotometric titration of macrocycle **7a** with $\text{Zn}(\text{OAc})_2$ in THF+4%EtOH; inset: Job's plot analysis (with $[\text{Zn}]_{\text{Total}} + [\text{Macrocycle}]_{\text{Total}} = 13.8 \mu\text{M}$ and χ_{Zn} : mol fraction of zinc atoms).

AFM and TEM imaging

Since spectroscopic (UV-Visible, NMR) and MS spectrometry experiments clearly indicate that both macrocycles **7a** and **7b** undergo aggregation in solution, we further investigated their self-assembly in the solid state by AFM and TEM microscopies. For AFM experiments, the samples were prepared on HOPG substrates. The macrocycles were deposited either by drop-casting or spin-coating solutions of **7a** or **7b** in CHCl_3 , toluene, THF or binary mixtures of them, and at different concentrations (see full details in the ESI, Tables S4 and S5). Regarding the technique of deposition, a quite smoother and more homogenous surface of the HOPG with reduced amount of residual small particles were usually obtained by using spin-coating instead of drop-casting, but no significant difference was observed regarding the final formation of the self-assembly. On the contrary, the size, shape and morphology of the fibers were strongly dependent of both the solvent and concentration. At concentrations above ca. 10–14 μM in all tested solvents (pure or mixtures), both macrocycle materials collapse into large amorphous domains and/or giant clusters on the surface. The same occurred at any concentration when THF was used as the uptake solvent. Using either CHCl_3 , toluene or mixtures of them, and a concentration of macrocycle in the range of 0.5–3 μM , we observed the formation of large bundles of fibers with lengths of several microns, variable width (up to ca. 40 nm) and heights (3–40 nm) for both **7a** and **7b** (Figures 7 and 8, respectively). According to our estimation of 3.0–3.2 nm for the diameter of a macrocycle particle (by DOSY-NMR and DFT-geometry optimized structures), and assuming a vertical orientation of the molecules over the surface, the height of the fibers measured by AFM fits well with mono- to multilayer- organizations (see AFM height profiles in the ESI, Figures S61–S68). The minimum height of 3.3–3.5 nm can be reasonably assigned to a monolayer of several microfibrils composed of stacked-macrocyces.

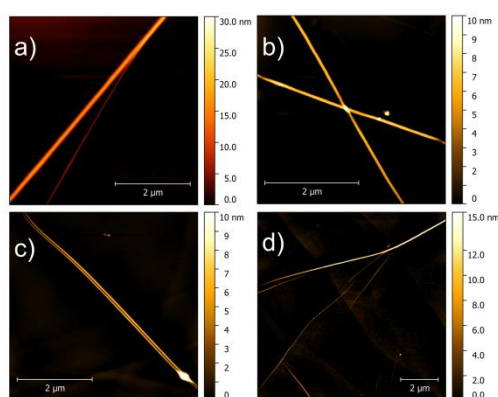


Figure 7. AFM images of macrocycle **7a** deposited on an HOPG surface: a) from a drop-casted solution in a 1:9 mixture of CHCl_3 /toluene ($1.4 \mu\text{M}$); b-d) from spin-coated solutions: b) $0.5 \mu\text{M}$ in toluene, c) $2.3 \mu\text{M}$ in toluene and d) $2.7 \mu\text{M}$ in a 1:4 mixture of CHCl_3 /toluene.

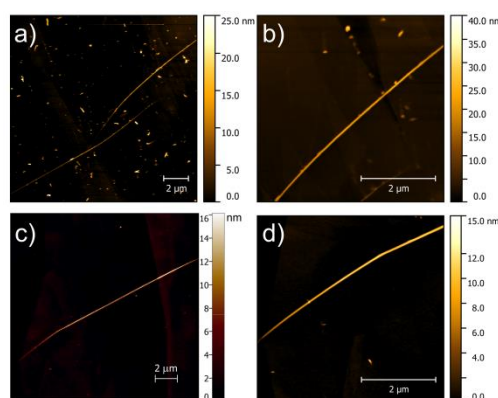


Figure 8. AFM images of metallomacrocycle **7b** deposited on HOPG surface from drop-casted solutions ($2.4 \mu\text{M}$) in: a, b) CHCl_3 /toluene (1:9); c, d) CHCl_3 .

For TEM experiments, all samples were prepared on carbon-coated grid substrates by drop-casting solutions of **7a** or **7b** in THF ($23\text{--}24 \mu\text{M}$), CHCl_3 ($23\text{--}24 \mu\text{M}$), or toluene ($12 \mu\text{M}$) (see details in the ESI, Tables S6-S11). As seen in Figures 9a-c, metal-free macrocycle **7a** gives long networks of interconnected bunch of fibers when drop-casted from a CHCl_3 solution, with length of several micrometers and width ranging from 7 nm to more than 80 nm. However, no self-organization was observed neither from toluene or THF solutions, collapsing into large clusters, droplets or amorphous domains under these conditions. In turn, the zinc-metallomacrocycle **7b** behaved far different than its metal-free analogue. First, fibers were observed from the three uptake solvents, and surprisingly, even when drop-casted from THF solution (Figure 9.e) although only few of them were observed in the latter conditions. Next, and in contrast with **7a**, only much shorter bundles of fibers ($<1 \mu\text{m}$) were obtained for **7b** (Figures 9.d-f), with width of 15–35 nm.

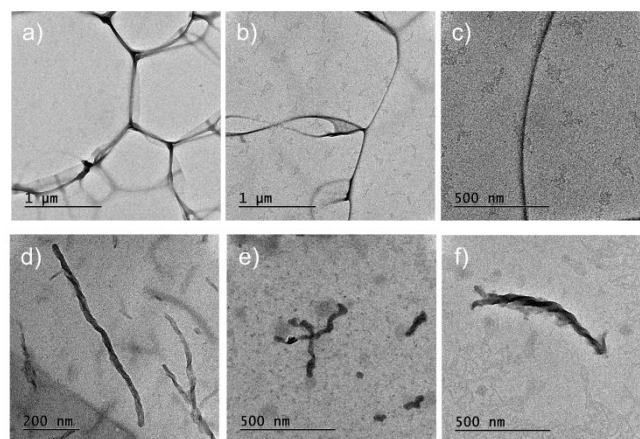


Figure 9. TEM images of **7a** (top; a-c) and **7b** (bottom; d-f) deposited onto a carbon-coated grid substrate; samples were prepared by drop casting solutions of a-c) **7a** in CHCl_3 [$23 \mu\text{M}$], d) **7b** in CHCl_3 [$24 \mu\text{M}$], e) **7b** in THF [$24 \mu\text{M}$], f) **7b** in toluene [$12 \mu\text{M}$], and then dried at ambient atmosphere for 24 h.

Unexpectedly, a close inspection of the TEM images revealed bundles of helical-type aggregates organized in “stick of liquorice”-shaped nanofibers (especially visible in Figures 9.d and 9.f). Such helical-shaped fibers were previously reported by MacLachlan and co-workers for dinuclear zinc(II) salphen complexes,^[49] but to our knowledge there is no such example reported in the case of salphen macrocycles.

Conclusions

A novel [3+3] salphen macrocycle (**7a**) having an unusual (inverted) design and an *ortho*-type substitution pattern was prepared. Metal-free (**7a**) and zinc-metallo (**7b**) macrocycles show weak to strong tendency to aggregate in solution, respectively, as evidenced by different spectroscopic techniques. This ability to self-assemble at the supramolecular level was confirmed in the solid state by AFM and TEM experiments, showing the formation of micrometer-sized fibers with diameter of several nanometers composed of stacked macrocycles.

Experimental Section

Synthesis and characterisation

Detailed experimental procedures, synthesis and characterization of the compounds (MS, NMR and UV-Visible spectra) are provided in the Supporting Information.

Diffusion-Ordered NMR Spectroscopy (DOSY)

DOSY $^1\text{H-NMR}$ experiments (500 MHz) were performed by the *Servicio Interdepartamental de Investigacion (SIdI)* at the *Autonoma University of Madrid* and were recorded on a Bruker TopSpin AV-500 spectrometer at 298 K. Mesitylene was used as internal reference for the estimation of the hydrodynamic radius of the macrocycle (See detailed procedures in

the Supporting Information). Data analysis and automatic DOSY processing 2D-transformation were performed using the MesReNova 14.1 software package, including the "Bayesian"- and newly implemented "Peak Heights fits"- DOSY Transform processing methods.

UV-Vis absorption and fluorescence spectroscopy

Steady-state absorption spectra were recorded on an *Agilent* Cary 50 UV-Visible spectrophotometer at room temperature, using either a standard 10 mm- (for low concentration range) or a 1 mm reduced path- (for high concentration range) UV cuvettes (QS). Fluorescence spectra were recorded on an *HORRIBA* Fluorolog[®]-3 spectrofluorometer using a 10 mm fluorescence UV cuvette (QS).

Atomic Force Microscopy (AFM)

AFM measurements were carried out in a commercial AFM system (Ntegra Prima, NT-MDT) in semicontact (dynamic) mode using scanning by sample configuration in ambient conditions. Rectangular silicon cantilevers HA_NC (NT-MDT) were used with a tip radius of 10 nm. Their nominal spring constant is 3.5 N/m and its resonance frequency is around 140 kHz. AFM samples were prepared by either drop-casting or spin-coating a solution of the macrocycles dissolved in CHCl₃, THF, toluene or mixtures CHCl₃/Toluene (1:9 or 1:4) at different concentrations onto HOPG substrates (See Tables S4 and S5 in the Supporting Information for details).

Transmission Electron Microscopy (TEM)

TEM experiments were performed by the *ICTS Centro Nacional de Microscopía Electrónica* at *Complutense University of Madrid*. TEM images were obtained on a JEM1400 Transmission Electron Microscope. Samples were prepared by drop-casting a solution of the macrocycles in CHCl₃ (23–24 μM), THF (23–24 μM) or toluene (11–12 μM) onto carbon-coated grids.

Geometry-optimized structures and DFT calculations

Molecular modelling was performed with the *Spartan'16* package (Wavefunction Inc.© 1991–2017) software for Windows. Minimized geometry-optimized structures (in vacuum) were obtained by DFT calculations at the B3LYP (6-31G*) level.

Acknowledgements

We are grateful for the financial support of the MINECO, Spain (CTQ2017-85393-P). IMDEA Nanociencia acknowledges support from the 'Severo Ochoa' Programme for Centres of Excellence in R&D (MINECO, Grant SEV-2016-0686). We thank Maite Alonso Pascual (MALDI-TOF MS), M^a Jesús Vicente Arana (ESI-MS) and María Dolores Penín Pérez (DOSY NMR) of the Servicio Interdepartamental de Investigación (SIdI) at the *Autónoma University of Madrid*, Dr. Patricia Pedraz (AFM) research staff at IMDEA Nanociencia Institute and Dr. Esteban Urones Garrote (TEM) from Centro Nacional de Microscopía Electrónica at Universidad Complutense de Madrid, for experiments and helpful discussions.

Conflicts of interest

The authors declare no competing financial interests.

Keywords: Macrocyclic ligands • Salphen • Schiff bases • Self-assembly • Supramolecular Chemistry

- [1] X. Liu, C. Manzur, N. Novoa, S. Celedón, D. Carrillo, J.-R. Hamon, *Coord. Chem. Rev.*, **2019**, *357*, 144-172.
- [2] S. Matsunaga, M. Shibasaki, *Chem. Commun.*, **2014**, *50*, 1044-1057.
- [3] S. Akine, *J. Inclusion Phenom. Macrocyclic Chem.*, **2012**, *72*, 25-54.
- [4] A. K. Crane, M. J. MacLachlan, *Eur. J. Inorg. Chem.*, **2012**, *2012*, 17-30.
- [5] J. Zhou, B. Wang, *Chem. Soc. Rev.*, **2017**, *46*, 6927-6945.
- [6] E. L. Gavey, M. Pilkington, *Coord. Chem. Rev.*, **2015**, *296*, 125-152.
- [7] S.-i. Kawano, Y. Ishida, K. Tanaka, *J. Am. Chem. Soc.*, **2015**, *137*, 2295-2302.
- [8] S.-i. Kawano, T. Hamazaki, A. Suzuki, K. Kurahashi, K. Tanaka, *Chem. - Eur. J.*, **2016**, *22*, 15674-15683.
- [9] S.-i. Kawano, M. Kato, S. Soumiya, M. Nakaya, J. Onoe, K. Tanaka, *Angew. Chem., Int. Ed.*, **2018**, *57*, 167-171.
- [10] J. Jiang, R. Y. Dong, M. J. MacLachlan, *Chem. Commun.*, **2015**, *51*, 16205-16208.
- [11] J. Zhang, L. Xu, W.-Y. Wong, *Coord. Chem. Rev.*, **2019**, *355*, 180-198.
- [12] K. Li, G. S. Ming Tong, Q. Wan, G. Cheng, W.-Y. Tong, W.-H. Ang, W.-L. Kwong, C.-M. Che, *Chem. Sci.*, **2016**, *7*, 1653-1673.
- [13] C.-M. Che, S.-C. Chan, H.-F. Xiang, M. C. W. Chan, Y. Liu, Y. Wang, *Chem. Commun.*, **2004**, 1484-1485.
- [14] G. Salassa, J. W. Ryan, E. C. Escudero-Adán, A. W. Kleij, *Dalton Trans.*, **2014**, *43*, 210-221.
- [15] P. A. Vigato, S. Tamburini, *Coord. Chem. Rev.*, **2004**, *248*, 1717-2128.
- [16] M. Martínez Belmonte, S. J. Wezenberg, R. M. Haak, D. Anselmo, E. C. Escudero-Adán, J. Benet-Buchholz, A. W. Kleij, *Dalton Trans.* **2010**, *39*, 4541-4550.
- [17] G. Consiglio, I. P. Oliveri, S. Failla, S. Di Bella, *Inorg. Chem.* **2016**, *55*, 10320-10328.
- [18] L. Leoni, A. Dalla Cort, *Inorganics* **2018**, *6*.
- [19] J. K.-H. Hui, P. D. Frischmann, C.-H. Tso, C. A. Michal, M. J. MacLachlan, *Chem. - Eur. J.*, **2010**, *16*, 2453-2460.
- [20] G. Salassa, A. M. Castilla, A. W. Kleij, *Dalton Trans.*, **2011**, *40*, 5236-5243.
- [21] A. J. Gallant, M. J. MacLachlan, *Angew. Chem., Int. Ed.*, **2003**, *42*, 5307-5310.
- [22] G. Salassa, M. J. J. Coenen, S. J. Wezenberg, B. L. M. Hendriksen, S. Speller, J. A. A. W. Elemans, A. W. Kleij, *J. Am. Chem. Soc.* **2012**, *134*, 7186-7192.
- [23] M. V. Escárcega-Bobadilla, G. A. Zelada-Guillén, S. V. Pyriin, M. Wegrzyn, M. M. D. Ramos, E. Giménez, A. Stewart, G. Maier, A. W. Kleij, *Nat. Commun.* **2013**, *4*, 2648.
- [24] G. A. Zelada-Guillén, M. V. Escárcega-Bobadilla, M. Wegrzyn, E. Giménez, G. Maier, A. W. Kleij, *Adv. Mater. Interfaces* **2018**, *5*, 1701585.
- [25] Y. Jin, C. Yu, R. J. Denman, W. Zhang, *Chem. Soc. Rev.*, **2013**, *42*, 6634-6654.
- [26] C. Yu, Y. Jin, W. Zhang, *chapter 3: Shape-persistent Macrocycles through Dynamic Covalent Reactions in Dynamic Covalent Chemistry: Principles, Reactions, and Applications*, (Eds.: W. Zhang, Y. Jin), John Wiley & Sons, Ltd, **2017**, pp. 121-163.
- [27] F. Mamiya, N. Ousaka, E. Yashima, *Angew. Chem., Int. Ed.*, **2015**, *54*, 14442-14446.
- [28] W. Zhang, J. S. Moore, *Angew. Chem., Int. Ed.*, **2006**, *45*, 4416-4439.

- [29] Z. J. Kinney, C. S. Hartley, *J. Am. Chem. Soc.*, **2017**, *139*, 4821-4827.
- [30] Z. J. Kinney, C. S. Hartley, *Org. Lett.*, **2018**, *20*, 3327-3331.
- [31] F. Ren, K. J. Day, C. S. Hartley, *Angew. Chem., Int. Ed.*, **2016**, *55*, 8620-8623.
- [32] A. Galán, E. C. Escudero-Adán, P. Ballester, *Chem. Sci.*, **2017**, *8*, 7746-7750.
- [33] M. Mastalerz, *Angew. Chem., Int. Ed.*, **2010**, *49*, 5042-5053.
- [34] M. Petryk, J. Szymkowiak, B. Gierczyk, G. Spólnik, A. Popenda, A. Janiak, M. Kwit, *Org. Biomol. Chem.*, **2016**, *14*, 7495-7499.
- [35] L. Zhang, L. Xiang, C. Hang, W. Liu, W. Huang, Y. Pan, *Angew. Chem., Int. Ed.*, **2017**, *56*, 7787-7791.
- [36] J. C. Lauer, W.-S. Zhang, F. Rominger, R. R. Schröder, M. Mastalerz, *Chem. - Eur. J.*, **2018**, *24*, 1816-1820.
- [37] G. Feng, W. Liu, Y. Peng, B. Zhao, W. Huang, Y. Dai, *Chem. Commun.*, **2016**, *52*, 9267-9270.
- [38] M. Mastalerz, *Chem. Commun.*, **2008**, 4756-4758.
- [39] S. Akine, T. Taniguchi, T. Nabeshima, *Tetrahedron Lett.*, **2001**, *42*, 8861-8864.
- [40] A. J. Gallant, J. K. H. Hui, F. E. Zahariev, Y. A. Wang, M. J. MacLachlan, *J. Org. Chem.*, **2005**, *70*, 7936-7946.
- [41] C. Ma, A. Lo, A. Abdolmaleki, M. J. MacLachlan, *Org. Lett.*, **2004**, *6*, 3841-3844.
- [42] S. Akine, D. Hashimoto, T. Saiki, T. Nabeshima, *Tetrahedron Lett.*, **2004**, *45*, 4225-4227.
- [43] C. T. L. Ma, M. J. MacLachlan, *Angew. Chem., Int. Ed.*, **2005**, *44*, 4178-4182.
- [44] A. J. Gallant, M. Yun, M. Sauer, C. S. Yeung, M. J. MacLachlan, *Org. Lett.*, **2005**, *7*, 4827-4830.
- [45] J. Jiang, M. J. MacLachlan, *Org. Lett.*, **2010**, *12*, 1020-1023.
- [46] J. K. H. Hui, M. J. MacLachlan, *Chem. Commun.*, **2006**, 2480-2482.
- [47] B. N. Boden, J. K. H. Hui, M. J. MacLachlan, *J. Org. Chem.*, **2008**, *73*, 8069-8072.
- [48] Y. Cohen, L. Avram, L. Frish, *Angew. Chem., Int. Ed.*, **2005**, *44*, 520-554.
- [49] J. K. H. Hui, M. J. MacLachlan, *Dalton Trans.*, **2010**, *39*, 7310-7319.

Entry for the Table of Contents

FULL PAPER



Dark side of the triangle. The synthesis and supramolecular organization of an (inverted) triangular-shaped [3+3] salphen macrocycle is reported. Metal-free and zinc-metallated macrocycles form nano- to micrometer- sized fibers in the solid state.

Maxence Urbani,* Tomas Torres*

Page No. – Page No.

A constrained and “inverted” [3 + 3] salphen macrocycle with an *ortho*-phenylethynyl substitution pattern

Accepted Manuscript